RSC Advances

PAPER

Cite this: *RSC Adv.*, 2016, **6**, 83973

Gas-phase synthesis of 3-carboethoxy-quinolin-4-ones. A comprehensive computational mechanistic study to uncover the dark side of the Gould–Jacobs reaction†

Ivana Malvacio,[ab] E. Laura Moyano[b] and D. Mariano A. Vera*[a]

Received 9th May 2016
Accepted 30th August 2016

DOI: 10.1039/c6ra11986g

www.rsc.org/advances

A set of 3-carboethoxy-quinolin-4-ones has been synthesized from diethyl 2-((arylamino)methylene) malonates through a Gould–Jacobs (G–J) cyclization using the flash vacuum pyrolysis (FVP) method. Mechanistic studies including calculations at first principles DFT and Coupled Cluster (CCSD(T)) levels of theory, along with insightful experiments, have been gathered to shed light on the complex multi-step process to afford quinolones. The G–J cyclization proceeded through a unimolecular process involving reactive species as iminoketenes, an azetinone and a quinolin-4(4*aH*)-one intermediates. The reaction was rate limited by a proton shift step in the pathway which leads to the final tautomeric product. In the gas phase pyrolysis of the starting malonates, along with the expected 3-carboethoxy-quinolin-4-ones, 3-unsubstituted-quinolin-4-ones were obtained, and the ratio between these products was strongly dependent on the nature of the arylamino group. In order to explain the deethoxycarbonylation reaction, DFT and *ab initio* calculations were also accomplished.

Introduction

Since the discovery of nalidixic acid in 1962, the quinolone structure has been considered of clinical and scientific interest.[1] The quinolone moiety is extensively used in a variety of pharmacologically active compounds for antibacterial,[2,3] anticancer[4] and antimalarial[5] uses among others.

Due to the large diversity of applications, different strategies have been used to synthesize the quinolone nucleus: from anthranilic acid derivatives and ketones, from ring closure of β-anilinoacrylates (Conrad–Limpach reaction) or from anilines and an ethoxymethylenemalonic ester.[6] The last one involves a condensation (Claisen condensation[7]) followed by an intramolecular cyclization (Camps cyclization[8]) known under the name of Gould–Jacobs (G–J) reaction from 1939.[9] Since its first application, this reaction started to be one of the most commonly used methodologies to obtain different quinolones[10] and quinolone-fused compounds as selenadiazoloquinolones,[11,12] pyrimidopyrrolopyrimidines,[13] pyridoquinoxalines,[14] *etc.*

Although the G–J reaction has been widely used as a successful synthetic approach in solution[15] and also under solvent-free conditions,[16] this complex multi-step reaction has never been studied in detail in the gas phase. There are only a few reports of application of this reaction under flow systems[17,18] and similar cyclization under flash vacuum systems.[19] Therefore, considering that the full G–J reaction mechanism including all the possible transition states (TS) and intermediates it is still not well known, we decided to carry out a typical G–J cyclization under flash vacuum pyrolysis (FVP) conditions. This type of gas-phase thermal reactions has proven to be an interesting methodology to study reaction mechanisms and also for synthetic purposes.[20–22] FVP consists in submitting a molecule to the application of high temperature (200–900 °C) during a short period of time ($\sim 10^{-2}$ s) under high vacuum ($\sim 10^{-2}$ to 10^{-1} Torr). This kind of solvent-less process allows the examination of reactive species such as carbenes, nitrenes, and radicals among others. Thus, FVP is an excellent technique for the study of intramolecular reactions such as eliminations and cyclizations with the resultant generation of products that cannot be prepared in conventional solution thermolysis. Moreover, from the mechanistic point of view, FVP reactions can easily be modeled since the inherent limitations of the theoretical solvent models are absent. Besides, performing the reaction in gas phase and vacuum, the focus can be placed on unimolecular processes over bimolecular ones or discrete interaction with solvent molecules.

Here we applied the FVP methodology as a novel approach to prepare 3-carboethoxy-6-substituted-quinolin-4-ones (**4a–f**,

[a]*QUIAMM-INBIOTEC – Department of Chemistry, School of Exact and Natural Sciences, National University of Mar del Plata, Mar del Plata, Buenos Aires, Argentina. E-mail: dmavera@yahoo.com*

[b]*INFIQC – Department of Organic Chemistry, School of Chemical Sciences, National University of Córdoba, Córdoba, Argentina*

† Electronic supplementary information (ESI) available: The information is organized in three parts: part I: substance characterization data; part II: thermochemistry details, additional table and figures, and part III: *xyz* coordinates of main stationary points discussed. See DOI: 10.1039/c6ra11986g

Scheme 1) from diethyl 2-((arylamino)methylene)malonates (**3a–f**). This transformation involved the G–J cyclization of malonates in gas phase, which has never been described before. An exhaustive computational mechanistic study of the whole reaction, starting from aniline (**1**) and diethyl-ethoxymethylenmalonate (**2**), was performed using DFT and *ab initio* (Coupled-Cluster) methods. The proposed steps were confirmed by locating the different intermediates and TS which lead to the final product. In addition, theoretical calculations were essential to explain the observed trend in the gas phase synthesis of **4** along with the formation of 6-substituted-quinolin-4-one (**6**) as a competitive product from a deethoxycarbonylation reaction.

Results and discussion

Flash vacuum pyrolysis reactions

In order to explore the intramolecular thermal cyclization of the G–J reaction, we decided to study the pyrolysis of diethyl 2-((arylamino)methylene)malonates **3a–f**. These precursors were satisfactory synthesized from anilines (**1a–f**) and diethyl-ethoxymethylenmalonate (**2**) applying microwave irradiation as it was previously reported (step 1, Scheme 1).[15]

As a first attempt, malonate **3c** was selected to optimize FVP conditions. Thus, pyrolysis were carried out at 250–500 °C (increasing 50 °C in each reaction) and $\sim 1 \times 10^{-2}$ Torr, during 1 hour. From 300 °C, conversion of substrate was quantitative and quinolones **4c** and **6c** were obtained as main products. Above 330 °C the formation of other products (like **5**, Scheme 1) was increased and the reaction mixture became complex. Taking into account these preliminary results, the temperature of 330 °C was chosen as the optimal value to perform the thermal study of remaining malonates (**3a–b**, **d–f**).

After performing FVP reactions, the treatment of the solid products with acetone gave rise to two different fractions: an insoluble fraction (**IF**) and a soluble one (**SF**). By using ^{1}H NMR it was determined that the **IF** was enriched with both quinolone derivatives (**4** and **6**), whereas the **SF** was enriched with **6**, containing also the un-reacted substrate (**3**) and other minor products (Table 1).

Regarding the results shown in Table 1, it is clear that the gas phase formation of quinolones **4a–f** was less efficient that its microwave-assisted synthesis in solution (diphenyl ether, 240 °C, 3 min) from the same starting malonates.[15] For the latter methodology, the yields of quinolone **4** ranged between 64–91%, whereas the yields obtained by FVP were only 5–44%. One of the reasons of the depleted generation of **4** can be attributed to the formation of the deethoxycarbonylated **6**, which was largely obtained in the pyrolysis of halogenated and nitro-malonates (**3c–f**). It is worthy to mention that compounds **6** were not produced in thermal reactions of **3** in solution (conventional or microwave-assisted procedures), which would indicate that FVP conditions favor the deethoxicarbonylation process at relatively low temperatures. A possible pathway for the formation of **6** could be *via* the anilinoacrylate **5**, which was detected in some FVP reactions depending on experimental conditions (Scheme 1). Indeed, the formation of similar intermediates was previously reported in the gas-phase decarboxylation of *N*-arylaminomethylene Meldrum's acid derivatives to give quinolones. Nevertheless, in these investigations high pyrolysis temperatures (around 600 °C) were required to afford the decarboxylation reaction.[23,24]

Theoretical mechanism study

Anilines **1b**, **1d** and **1f**, which have different electronic substituents in *para* position (an electron donor, a halogen and an electron withdrawing group, respectively) were selected as representative substrates to perform the theoretical study of the G–J mechanism. The first step involved the addition of the aniline **1** to malonate **2** followed by ethanol elimination to provide the anilinomethylenemalonic ester **3** (Scheme 2). A summary of the free energy reaction profile is shown in schematic form in Fig. 1 for the case of the bromo-derivative **1d**.

A productive complex **I** between substrates **1** and **2** was stabilized by a strong hydrogen bond between the nitrogen center of the aniline and one of the carbonyl oxygen of malonate. Then, a nucleophilic attack of the aniline to the vinylic

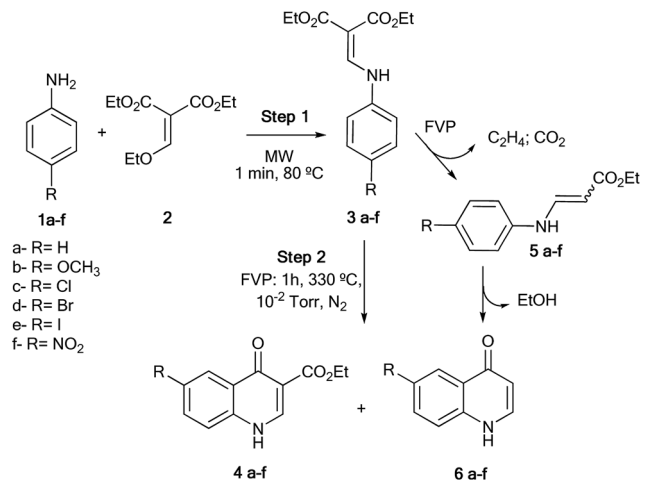

Scheme 1 Formation of quinolone derivatives under FVP.

Table 1 Composition of pyrolyzates in the FVP of malonates **3a–f**

		Product composition						
		IF[a] (%)		**SF**[a] (%)				
Substrate	R	**4**	**6**	**3**	**4**	**6**	Other	**IF : SF**[b]
3a	H	93	7	23	—	42	35	63 : 37
3b	OCH_3	95	5	12	46	25	17	60 : 40
3c	Cl	78	22	1	47	51	—	60 : 40
3d	Br	87	13	2	—	65	33	51 : 49
3e	I	86	14	22	—	67	11	56 : 44
3f	NO_2	23	77	8	—	78	14	35 : 65

[a] **IF**: insoluble fraction (composed by **4** and **6**), **SF**: soluble fraction (composed by **3**, **4**, **6** and others). [b] Molar ratio calculated from the analysis of ^{1}H NMR spectrum.

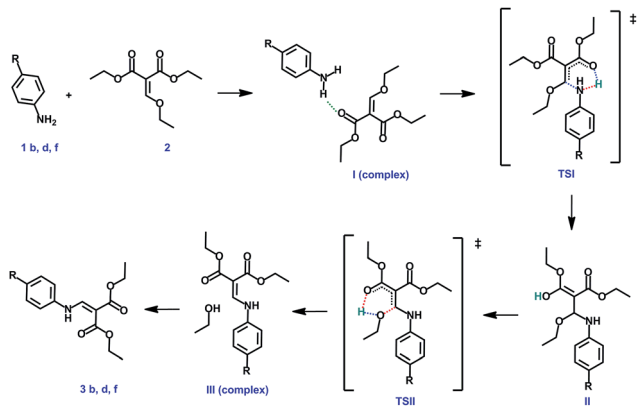

Scheme 2 First step of the G–J reaction mechanism.

carbon of malonate gave an enol intermediate **II**, through a transition state (**TS-I**) with a barrier of 23.5 kcal mol^{-1}. Next up, **II** easily cleaves with the elimination of an ethanol molecule, passing through a TS similar to the previous one (**TS-II**, 24.2 kcal mol^{-1}) affording product **3** (Fig. 1a). For all substrates, the profiles for this step were found to have very similar free energies ($\Delta\Delta G \sim 2$ kcal mol^{-1}, Fig. 1b).

By comparing the three different substituents, the lowest **TS-II** energy was obtained for reaction of **1b**, where methoxy group in the aniline ring seems to favor the attack of this amine to the vinylic carbon of **2** (further details about total energies in atomic units for all the steps and additional figures and computational details are reported in the ESI,† part II).

The second step of the mechanism involves the cyclization of **3** to give **4** (Scheme 3). Thus, once the product **3** was formed, it can interconvert in different conformers from which either an ethanol or an ethene molecule could be eliminated, thus leading to two possible pathways: formation of quinolin-4-one **4**, hereafter referred as path A (Scheme 3), or the formation of deethoxycarbonylated-quinolin-4-one **6**, labeled path B (Scheme 4).

According to our calculations and previous crystallographic data,[25] the most stable conformer of **3** is the one which establishes a hydrogen bond between the nitrogen of aniline and the carbonyl of the ester group. However, at the beginning of path A we observed the interconversion to the conformer **A-IV**, which establishes a hydrogen bond between the nitrogen of aniline and the oxygen of one ethoxy instead of carbonyl group (Scheme 3). Such conformation allows the initial ethanol detachment, which was found to be endergonic and concerted with the proton transfer from the aniline; thus yielding a loose complex between the iminoketene intermediate **A-V** and the ethanol (hereafter and for the sake of brevity, most of the calculated loose complexes will be generally omitted from the discussion). All reasonable fates of this ketene were studied by considering isomerizations and different ring closures (not shown) nevertheless, only the two lowest energy paths will be discussed.

In these paths, **A-V** could either cyclize to azetinone **A-VI′** or interconvert by the indicated bond rotation (**TS-A-V**) to its isomeric ketene **A-VI**, which finally leads to the six-membered ring closure (Scheme 3). At the same time, the azetinone **A-VI′** could also reach **A-VI** through a ring opening-closure TS (**TS-A-V′**) which was 2.6 kcal mol^{-1} lower than **TS-A-V**, indicating that both pathways are possible in practice. The free energy profile at CAM-B3LYP/6-311+G(d,p) level of theory is shown in Fig. 2 for **3d**. Moreover, the free energies obtained for all species in Scheme 3 are summarized on Table 2 for the three different substituents.

The analysis of the electrostatic potential (Fig. 3) evidenced that the ketene carbon of **A-V** was a strong electrophile; this fact could justify the two possibilities of reaction of **A-V**: (i) cyclization to azetinone **A-VI′** and (ii) direct isomerization to **A-VI**, which in the next step could be suitable for the attack to the phenyl ring leading to the quinolin-4(4a*H*)-one intermediates intermediate **A-VII**.

At this point, it is worth to mention that path A was also calculated for all derivatives at the Coupled Clusters level of

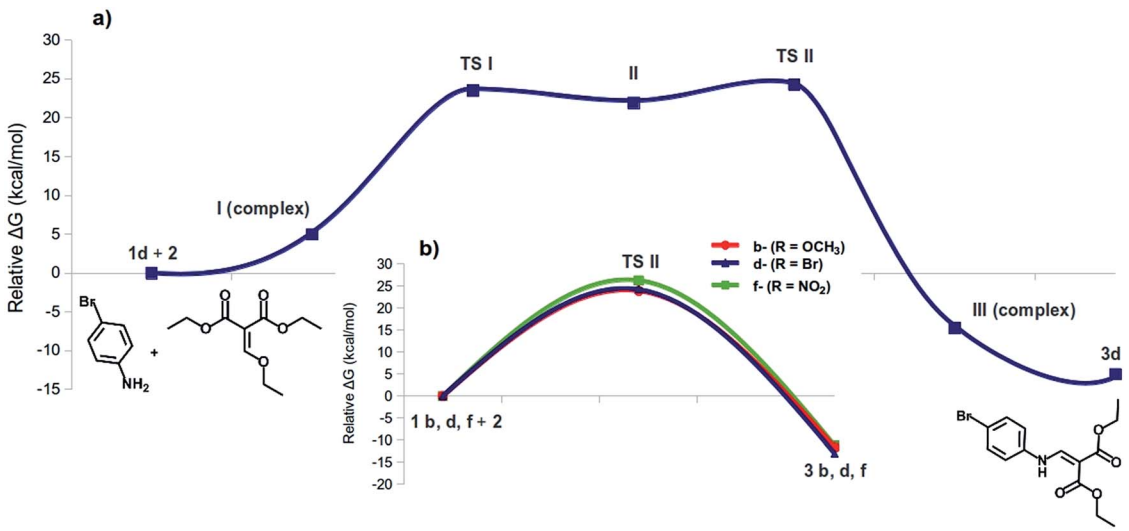

Fig. 1 (a) Free energy profile of aniline **1d** at CAM-B3LYP/6-311+G(d,p) level for the first step of the reaction. In the inset (b) comparison of the three substrates (**1b**, **1d** and **1f**), including reactants, highest TS and product **3** at the same level of theory.

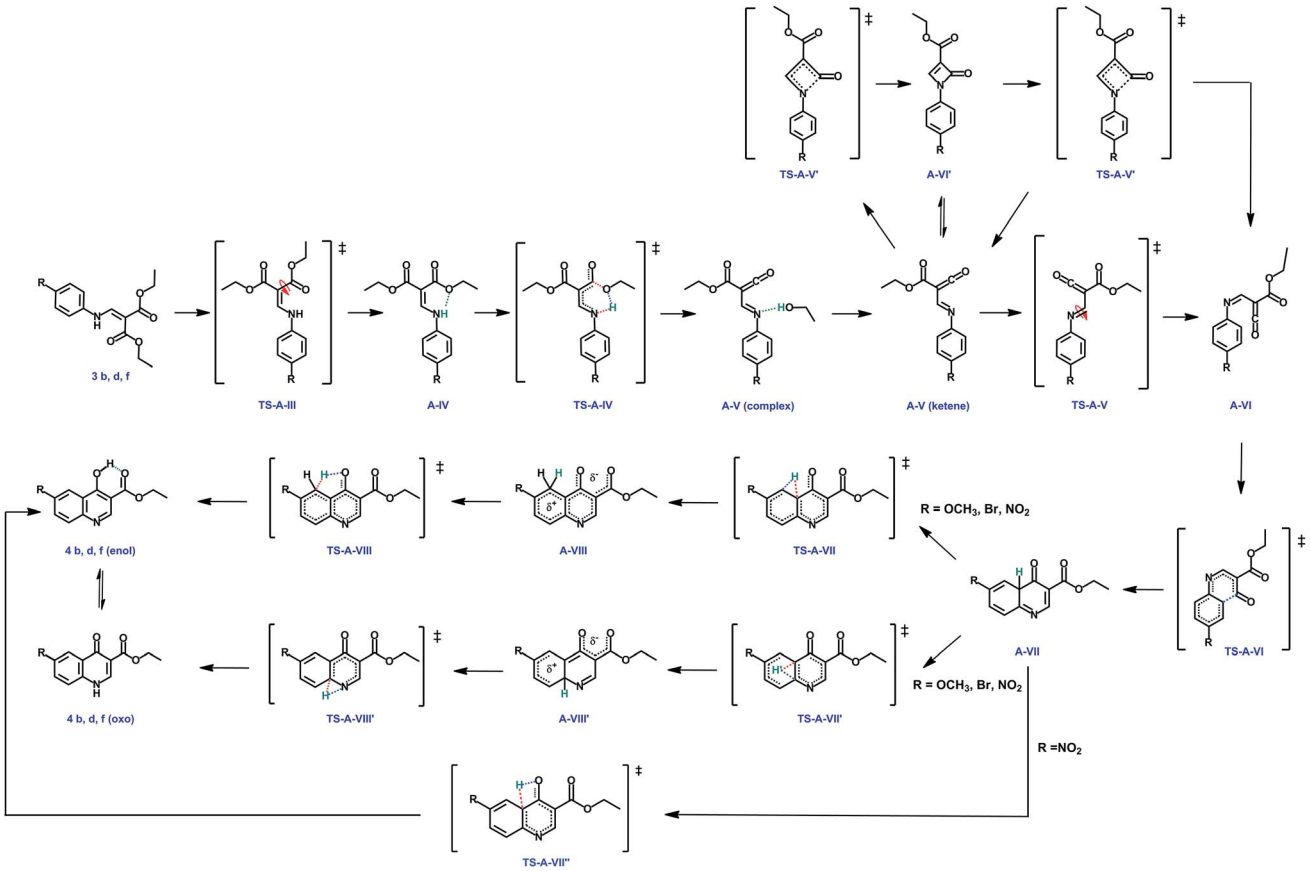

Scheme 3 Main reaction (path A) leading to the formation of quinolone **4**.

theory to improve the quality of calculations; the superimposed profiles for the three substituents are shown (starting from **A-V**) on Fig. 4. For the three derivatives the agreement between the functional and the higher level energy improvement at CCSD(T) were very good; the comparison of energy profiles at CAM-B3LYP and CCSD(T) level of theory is depicted in Fig. S3 on the ESI.† The calculations revealed that all derivatives display similar reaction coordinates. The main differences between

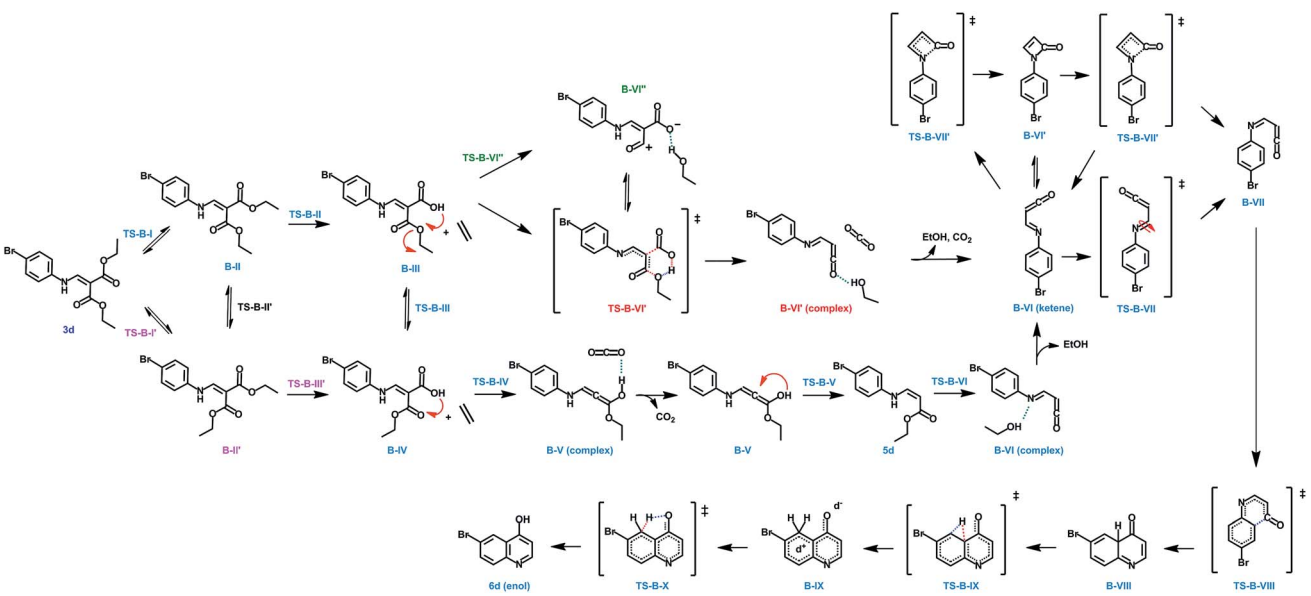

Scheme 4 Mechanism proposed for the formation of quinoline **6d** (path B).

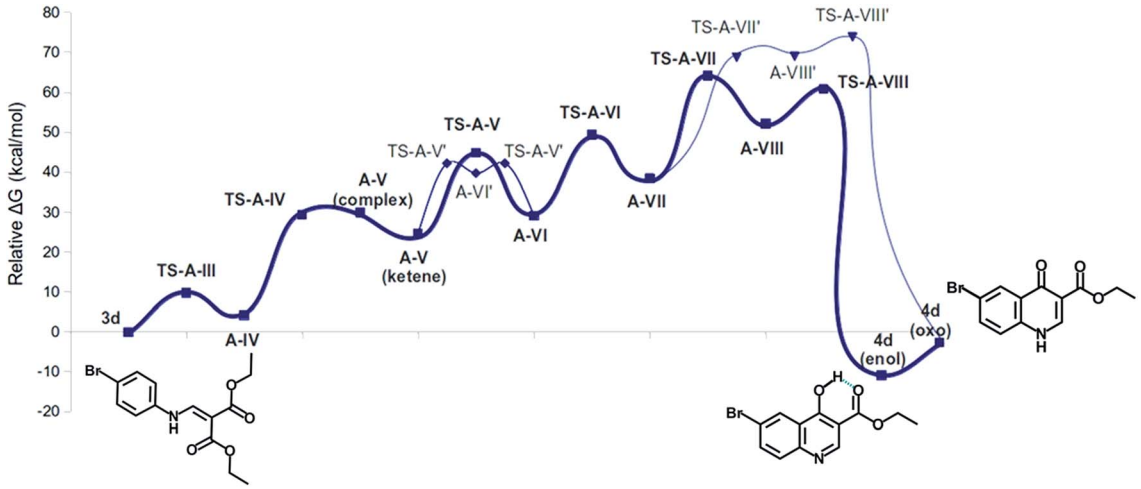

Fig. 2 Free energy profile for the reaction path A for **3d** at the CAM-B3LYP/6-311+G(d,p) level of theory.

Table 2 Summary of relative free energies for the main stationary points discussed on Scheme 3[a]

	CAM-B3LYP			CCSD(T)		
	R =			R =		
Path A	OMe	Br	NO_2	OMe	Br	NO_2
3b, d or **f**	0.00	0.00	0.00	0.00	0.00	0.00
A-IV	4.81	5.44	5.43			
TS-A-IV	35.78	35.83	35.74		29.03	
A-V complex	31.51	32.00	31.68			
A-V	25.86	25.88	25.72	22.99	22.65	22.56
TS-A-V	47.74	46.12	43.47	48.50	46.72	44.97
A-VI	29.90	30.38	29.57	24.80	24.75	24.71
TS-A-VI	47.98	50.70	52.32	43.28	45.75	47.07
A-VII	36.23	39.72	41.92	30.04	32.91	34.43
TS-A-VII	60.25	65.49	70.12	59.43	62.84	67.17
A-VIII	41.66	53.46	61.56	42.26	52.24	57.54
TS-A-VIII	51.98	62.21	68.29	50.94	60.38	64.75
4 (enol)	−9.61	−9.61	−8.94	−10.07	−10.60	−10.24
4 (oxo)	−1.75	−1.40	5.75	−1.56	−1.84	−1.37
TS-A-V′	43.31	43.49	42.75	40.58	41.96	41.33
A-VI′	40.81	41.01	40.69	38.68	38.11	38.17
TS-A-VII′	61.76	70.33	76.38			71.18
A-VIII′	59.75	70.05	76.92			70.23
TS-A-VIII′	68.92	75.21	79.21			73.29
TS-A-VII′ (direct)			81.68			78.32

[a] ΔG^0 relative to reactants **3b**, **3d**, and **3f** respectively; all energies are expressed in kcal mol^{-1}.

them were: (i) the activation barrier associated with **TS-A-V** was higher for methoxy derivative **3b** than for the bromo and nitro derivatives, (ii) the electrophilic attack of the ketene carbon to the phenyl ring leading to the six-membered ring closure to form **A-VII** was found easier for **3b** than for the bromo and nitro derivatives with higher **TS-A-VI** barriers and (iii) in all cases the activation barriers for proton shifts in the quinolone ring *via* **TS-A-VII** and **TS-A-VIII** (see also Scheme 3) were higher than any previous isomerization and/or ring closure steps, it being clearly

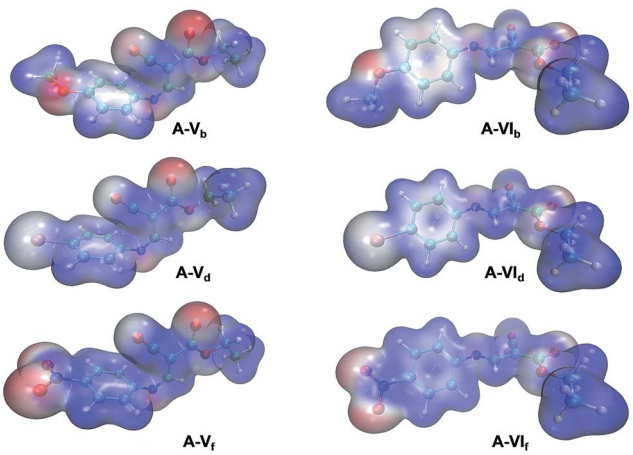

Fig. 3 Molecular electrostatic potentials colored on an electron isodensity surface of 0.01 a.u. for the isomeric ketenes. Color ranges from red (−0.1) to blue (+0.1 a.u.). Ketenes **A-V$_b$** and **A-VI$_b$** come from **3b** (R = OMe), ketenes **A-V$_d$** and **A-VI$_d$** come from **3d** (R = Br) and ketenes **A-V$_f$** and **A-VI$_f$** come from **3f** (R = NO_2).

higher in the case of the nitro (**3f**) than for bromo- and methoxy-derivatives. In the following step, the ketene **A-VI** afforded the benzo-annulation reaction to produce **A-VII** (Scheme 3). In this transformation the electronic effect of aryl substituents was clearly observed. Thus, the higher electron density on the phenyl ring for R = OCH_3 (Fig. 3a) would favor the electrophilic attack of the ketene **A-VI** giving the cyclization to form the intermediate **A-VII**. Therefore, the order of reactivity for **A-VI** to **A-VII** according to the substituents on the phenyl ring was: R = OCH_3 > Br > NO_2 (see the comparison of the three energy profiles, from **A-VII** to the final products on Fig. 4).

It is interesting to note that the cyclization step would be rate controlling under solvent conditions since once **A-VII** is formed; it would readily tautomerize to either its oxo or enol aromatic forms (*i.e.* the final products) through bimolecular processes. However, under extremely low pressure as it was done in FVP

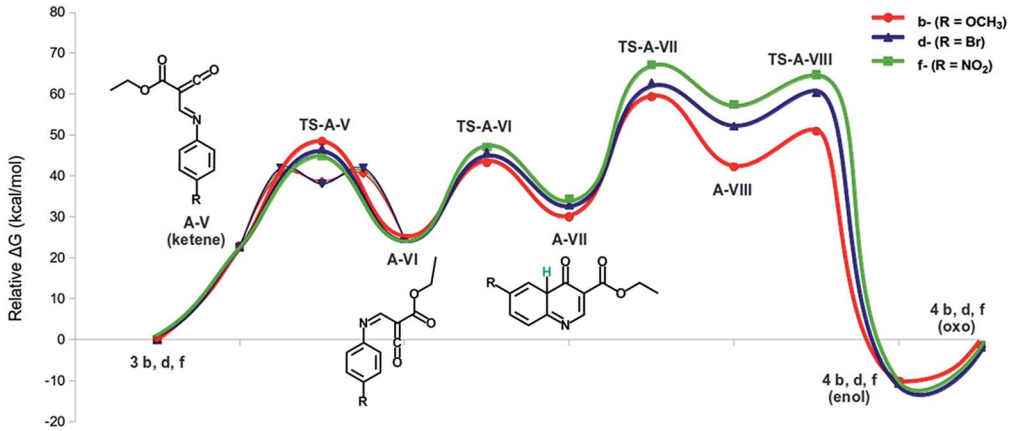

Fig. 4 Free energy profiles for the path A, detailed after the iminoketene **A-V** formation from **3b**, **d**, **f** at CCSD(T) level of theory.

reactions, the only path for tautomerization of **A-VII** was actually the intramolecular proton shift.

According to the mechanism here proposed, the gas phase tautomerization of **A-VII** to enol **4** could be produced through two consecutive H-shifts: [1,2]H-migration to give **TS-A-VII** and then [1,4]H-migration to form **TS-A-VIII**. The 3D-structures for this sequence of intermediates and TS are summarized on Fig. 5 for the case of **3d** (R = Br). Alternatively, the transformation of **A-VII** to oxo tautomer **4** could occur through two consecutive [1,2]H-migrations, through **TS-A-VII′** and **TS-A-VIII′**; however, this possibility was the pathway with higher energy (Fig. 2).

The direct [1,3]H-migration from C4a to the carbonyl oxygen was also considered. In this case we were not be able to locate the transition-state structures involved in this process for quinolines coming from **3a** and **3d**; however for derivative **3f** a four-membered TS was found (**TS-A-VII″**). The calculations indicated that this TS was significantly higher in energy (11.6 kcal mol^{-1} higher than **TS-A-VII**). From the calculations, the H-shifts in **TS-A-VII** and **TS-A-VIII** were influenced by the substituents in the quinolone ring. Thus, the TS structure **TS-A-VII** for quinoline **3b** was predicted to be 9.9 kcal mol^{-1} lower in energy than **TS-A-VII** for **3f**.

Also for the sigmatropic shift *via* **TS-A-VIII**, the TS associated with **3b** was lower in energy than for the other quinolines (10.2 and 16.3 kcal mol^{-1} lower than for **3d** and **3f**, respectively). Therefore the activation barriers for these transitions were in the following order of substituents: OCH_3 < Br < NO_2 (Fig. 4).

By analyzing the electrostatic potentials of intermediate **A-VII** it could be demonstrated that the hydrogen involved in this TS has a positive charge density (Fig. 6). Thus, considering this proton has to migrate to C5, in α-position to the substituents R, it became clear that the electron rich substituents favored this transposition while it was disadvantaged by electron withdrawing substituents. This effect may also be the reason why direct [1,3]H-shift from the C4a to the carbonyl oxygen to form

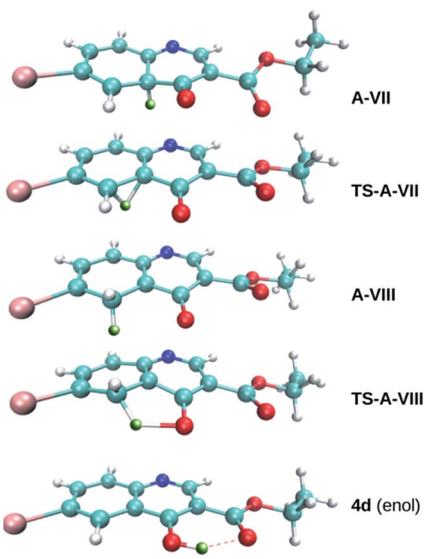

Fig. 5 Structures of the stationary points found for the lowest free energy pathway for the sequence **A-VII** to **4d** (the TS for the OH rotation to form an H-bond is omitted).

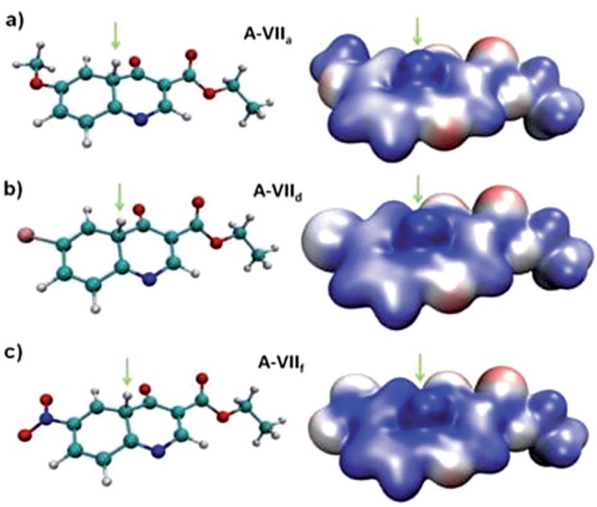

Fig. 6 Structure and electrostatic potential of the intermediate **A-VII**: (a) **A-VII$_b$** come from **3b** (R = OMe), (b) **A-VII$_d$** come from **3d** (R = Br) and (c) **A-VII$_f$** come from **3f** (R = NO_2).

enol **4**, was only observed for the nitro derivative. This pathway is not further discussed here since it was the way with the highest activation energy, probably due to the fact that [1,3]H-shifts are thermally prohibited[26] (see the energy profile for nitro derivative in Fig. S4 of ESI†). According to Fig. 2 and 4, **TS-A-VII** could be thought as the rate-determining TS under FVP conditions, since it is the highest TS in energy. However, as it was previously reported by Kozuch *et al.*, here it might be thought that the reaction was controlled by a rate-determining zone, which could be defined by two consecutive steps, from intermediate **A-VII** to the final product **4**. This rate-determining region would include the highest transition states **TS-A-VII** and **TS-A-VIII**, the last one being an irreversible step and both of them strongly affected by the electronic nature of the ring substituents.[27]

It is important to mention that intermediates like **A-VI** and **A-VII** have been reported particularly in the pyrolysis of Meldrum's acid derivatives.[18,23] These processes were previously proposed to have high activation barriers in similar reactions steps. However, to the best of our knowledge, no-one could describe and characterize the process in detail and the intramolecular proton transfer described above has never been studied in depth. Indeed, the researchers that have performed theoretical calculations of this reaction involving 6π electrocyclization to afford quinolone nuclei, through intermediates like **A-VII**, could not find the TS corresponding to the H-shift described for the tautomerization step.[17,28] This fact, was another motivation to study the mechanism at a higher level of theory (CCSD(T)) in order to confirm the energetics of the proposed steps. Once studied the path A, the possible reaction mechanism leading to the formation of **6** was also studied, this mechanistic way is named path B and is represented in Scheme 4 (the relative free energies are summarized on ESI Table S1,† similar to Table 2 for the main path A).

Due to the high temperatures raised in the FVP reactions, it would be possible to achieve a higher TS than for the release of ethanol (described in the path A), corresponding to the elimination of ethene (**TS-B-II** or **TS-B-III′**, Fig. 7 and Scheme 4).

Once the ethene molecule was released, the intermediate formed (**B-III**) could either lose ethanol followed by CO_2 elimination in two consecutive steps (**TS-B-VI″** and **B-VI″**, green curve in Fig. 7) or in a concerted way (**TS-B-VI′**, red curve in Fig. 7). Another possibility could be the CO_2 release from **B-IV** to achieve the cumulene **B-V** followed by formation of **5** (experimentally detected), which can eliminate ethanol to give the iminoketene intermediate (**TS-B-VI**, cyan curve Fig. 7). The fact that **5** was detected in the FVP experiments, and also this compound was the thermodynamically most stable intermediate (−5.3 kcal mol^{-1}, Fig. 7), let us to the study of path B considering the loss of carboethoxy group from malonate **3**, instead of thinking about deethoxycarbonylation of quinolone **4**. In addition, it is known that elimination of carboxy groups in gas phase requires very high temperatures (600–800 °C) in most of the organic compounds.[20]

The TS which gave rise to **5** was the most energetic (**TS-B-V**) along this pathway, and it was also higher than **TS-A-VII** (Fig. 2 and Scheme 3), probably because the [1,3]H-shift required in the cumulene intermediate (Scheme 4). Therefore, and due to the irreversibility of this step, the formation of **5** could be candidate for the rate-determining state for path B. Henceforth, in the formation of quinolone **6**, the mechanism continued in an analogous way that the calculated for path A, *i.e.* through a ketene intermediate (**B-VI**), ring closure and successive H-shifts (Scheme 4 and Fig. 7).

Besides the high energy of the **TS-B-V**, and even if it were avoided by following an alternative path, the first ethene elimination had also a very high energy. These TSs were similar and lied between 62 and 66 kcal mol^{-1} (Fig. 7 and Table 2), with little difference between the three substituents. In contrast, the controlling steps on path A, *i.e.* the proton-shift tautomerization steps are more sensitive to the substituent (Fig. 4). In the case of the most reactive R = OMe, the tautomerization step **TS-A-VII** which controlled path A was at 60.2 kcal mol^{-1}; this explains the abundance of **4b** as clear main product in the case of **3b**. On the opposite edge, for the case of R = NO_2, the corresponding tautomerization TS was 70.1 kcal mol^{-1}, this allowing path B to

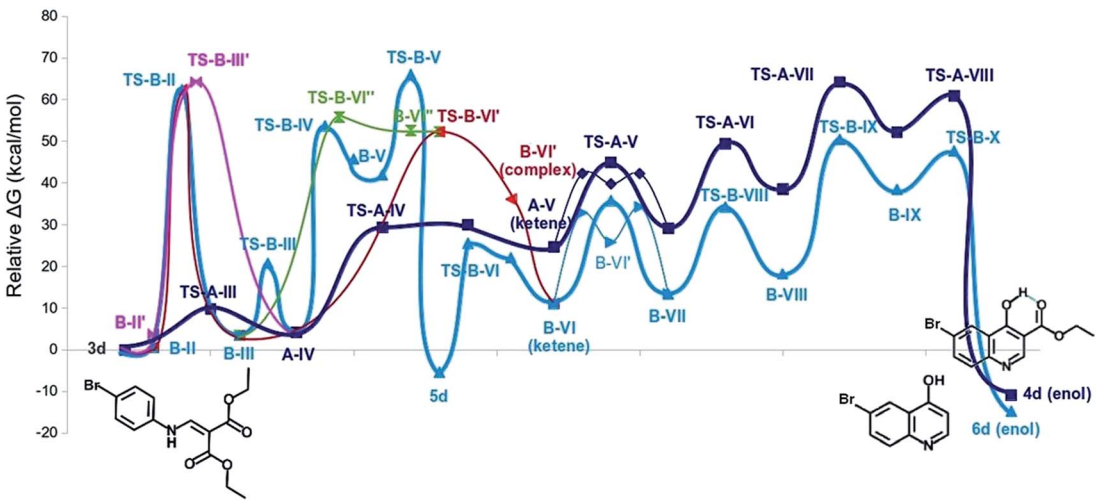

Fig. 7 Comparison between the free energy profiles along the path B (colors according to Scheme 4) and the path A (dark blue) for **3d**.

be competitive. Again in good agreement with the experiments, the nitro derivative was the poorest in its **4 : 6** ratio (actually, **6** was more abundant than the desired product **4** in this case).

As well as the product distribution **4 : 6** ratio, the above comparison between the TS on each path can explain the unique reactivity observed in FVP conditions. The ratio of both quinolones was determined by the height of the tautomerization TSs on path A (**TS-A-VII**) which are comparable to several TSs above 50 kcal mol^{-1} on path B. However, the critical ethene detachment on path B (with more than 60 kcal mol^{-1} TS) will occur for each substituent either in gas phase or a solvent media. But the tautomerizations (above 50 kcal mol^{-1}) on path A would not present an important barrier if the reaction had been made in solvent media. Under such condition, the highest TS in path A would be far below any TS in the path B and consequently this path could not have been competitive.

Conclusions

A typical G–J reaction was performed from anilines (**1**) and diethyl ethoxymethylenmalonate (**2**) combining microwave irradiation, for the formation of diethyl-phenylaminomethylenemalonates (**3**) and, for the first time, FVP of these malonates to accomplish their cyclization to quinolin-4-ones. In a surprising development, in the gas phase reactions of **3**, the deethoxycarbonylated-quinolone (**6**) (besides the expected carboethoxy-quinolone (**4**)) was obtained.

In order to understand the observed trend, first principles calculations were performed to study the complete reaction mechanism in-depth. Once **3** was formed, the reaction proceeded in one or another fate depending on whether only one ethanol molecule was released, or ethene and carbon dioxide followed by ethanol were lost, giving **4** and **6** respectively. In both cases an iminoketene (**A-V** or **B-VI**) was found as a key intermediate. When such ketene was attacked by the phenyl ring, a quinolone-like intermediate was formed (**A-VII** or **B-VIII**), which tautomerized to the final product through two consecutive H-shifts. Surprisingly, the most energetic TS along the reaction were found to be these hydrogen migrations, which could be the rate-determining zone in the gas phase process. For the first time, in the present study, it was possible to characterize all TS of the process calculating their energies with a high accuracy CC method. The effect of the substituents on the starting aniline were also analyzed and discriminated according to the role they played in each step of the whole mechanism.

Pyrolysis of malonate **3** proceeded through two competitive reactions that led to the formation of quinolones **6** and **4**. The aniline acrylate **5** was found to be a key intermediate to understand the deethoxycarbonylation process from **3**, which occurred before the ring closure towards quinolone formation.

Experimental

General procedure for the synthesis of diethyl 2-((phenylamino)methylene) malonates (3a–f)

Anilines **1a–f** (0.25 g, 2.69–1.14 mmol) and diethyl ethoxymethylenmalonate (0.54–0.23 mL) were irradiated in a Microwave Monomode CEM Discovery equipment during 1 min at 80 °C using dynamic method in a sealed vessel according to procedure described in our previous paper.[15]

General procedure for the study of diethyl 2-((phenylamino) methylene) malonates (3a–f) cyclization under FVP conditions

FVP reactions were carried out in a Thermolyne 21100 furnace using a vycor glass of 30 cm long and a 1.2 cm i.d. reactor. Temperatures were 250–500 °C, being 330 °C the optimized temperature, pressures of 10^{-2} Torr, contact times were 10^{-2} s, total reaction time 1 h and sample amounts were ~20 mg (see ESI† for equipment details). After the experiments were completed, the pyrolysate was collected in a liquid N_2 trap and extracted with acetone. The solid product/s was/were filtered. Finally, both solid and soluble products were submitted to conventional analysis (^{1}H NMR, ^{13}C NMR and GC/MS). NMR spectra of 4-oxo-1,4-dihydroquinoline-3-carboxylates **4a–f** were identical to previously reported in the conventional and microwave-assisted preparation.[15] Meanwhile, quinolinones **6a–f** were also characterized by their NMR spectra which agreed with previously described in literature.[29] Compound ethyl 3-((4-chlorophenyl)amino)acrylate (**5c**) was identified from the reaction mixture by GC/MS (see ESI†).

Computational methodology

The whole potential energy surface exploration was carried out using the Gaussian 09 package for the DFT calculations.[30] All the relevant stationary points along the main path (called path A within the discussion) as well as key points on side path B were also calculated using the PQS 4.0 software,[31] using its implementation of the Coupled Clusters theory,[32] at the CCSD(T) level,[33] within its CORR module.[34] In the case of the bromo derivatives, both the main path A and path B were treated at the CCSD(T) level. All the structures of reactants, TSs, intermediates, and products were optimized in the gas phase at the CAM-B3LYP/6-311+G(d,p) level of theory and characterized by means of the Hessian diagonalization and further harmonic frequencies analyses for obtaining zero point and thermal corrections to the energy, enthalpy and free energy.[35] The CCSD(T) energies were computed at those optimized geometries. In relevant cases, IRC simulations were started from the TS computed modes, using mass weighted coordinates. The CCSD(T) calculations were done with frozen core for internal electrons, by considering them as core if their energies were at least 2.9 eV below the HOMO. Compounds on Table 2 are ground state singlets with net charge of 0. Visualization and graphics rendering was done with Gabedit 2.4.7 (ref. 36) and VMD 1.8.9.[37,38]

Acknowledgements

This work was supported in part by MINCyT and FONCYT, together with the National Research Council of Argentina (CONICET). I. Malvacio acknowledges the receipt of a scholarship from the CONICET.

Notes and references

1 A. Emmerson and A. Jones, *J. Antimicrob. Chemother.*, 2003, **51**, 13.
2 N. Kumar, D. Dhivya and B. Vijayakumar, *Int. J. Novel Trends Pharm. Sci.*, 2011, **1**, 23.
3 V. Milata, R. M. Claramunt, J. Elguero and P. Zálupský, *Targets Heterocycl. Syst.*, 2000, **4**, 167.
4 J. Sun, H. Zhu, Z.-M. Yang and H.-L. Zhu, *Eur. J. Med. Chem.*, 2013, **60**, 23.
5 R. Beteck, F. Smit, R. Haynes and D. N'Da, *Malar. J.*, 2014, **13**, 339.
6 R. Reitsema, *Chem. Rev.*, 1948, **43**, 43.
7 L. Claisen, *Ber. Dtsch. Chem. Ges.*, 1897, **20**, 655.
8 R. Camps, *Arch. Pharm.*, 1901, **239**, 591.
9 R. Gould and W. Jacobs, *J. Am. Chem. Soc.*, 1939, **61**, 2890.
10 K. Plevová, K. Briestenská, F. Colobert, J. Mistríková, V. Milata and F. Leroux, *Tetrahedron Lett.*, 2015, **56**, 5112.
11 M. Bella, M. Schultz, V. Milata, K. Koňariková and M. Breza, *Tetrahedron*, 2010, **66**, 8169.
12 M. Bella and V. Milata, *ARKIVOC*, 2014, **5**, 181.
13 N. Desai, *J. Heterocycl. Chem.*, 2006, **43**, 1343.
14 J. Saloň, V. Milata, N. Prónayová and J. Leško, *Collect. Czech. Chem. Commun.*, 2001, **66**, 1691.
15 I. Malvacio, D. Vera and E. Moyano, *Curr. Microwave Chem.*, 2014, **1**, 52.
16 P. Černuchová, G. Vo-Thanh, V. Milata and A. Loupy, *Heterocycles*, 2004, **64**, 177.
17 D. Cantillo, H. Sheibani and O. Kappe, *J. Org. Chem.*, 2012, **77**, 2463.
18 L. Lengyel, T. Nagy, G. Sipos, R. Jones, G. Dormán, L. Ürge and F. Darvas, *Tetrahedron Lett.*, 2012, **53**, 738.
19 L. Lengyel, G. Sipos, T. Sipőcz, T. Vágó, G. Dormán, J. Gerencsér, G. Makara and F. Darvas, *Org. Process Res. Dev.*, 2015, **19**, 399.
20 R. Brown, in *Pyrolytic Methods in Organic Chemistry: Application of Flow and Flash Vacuum Pyrolytic Techniques*, ed. H. Wasserman, Academic Press Inc., New York, 1980.
21 P. Lucero, W. Peláez, Z. Riedl, G. Hajós, E. Moyano and G. Yranzo, *Tetrahedron*, 2012, **68**, 1299.
22 G. Yranzo and E. Moyano, *Curr. Org. Chem.*, 2004, **8**, 1071.
23 A. Gaber and H. McNab, *Synthesis*, 2001, **14**, 2059.
24 H. Briehl, A. Lukosch and C. Wentrup, *J. Org. Chem.*, 1984, **49**, 2772.
25 V. Langer, E. Scholtzová, V. Milata and T. Solcan, *Acta Crystallogr., Sect. C: Cryst. Struct. Commun.*, 2007, **63**, 552.
26 R. Woodward and R. Hoffmann, in *The Conservation of Orbital Symmetry*, Verlag Chemie GmbH Academic Press Inc., Weinhein, 1970.
27 S. Kozuch and J. Martin, *ChemPhysChem*, 2011, **12**, 1413.
28 L. George, K.-P. Netsch, G. Penn, G. Kollenz and C. Wentrup, *Org. Biomol. Chem.*, 2006, **4**, 558.
29 B. Margolis, K. Long, D. Laird, J. Ruble and S. Pulley, *J. Org. Chem.*, 2007, **72**, 2232.
30 M. Frisch, G. Trucks, H. Schlegel, G. Scuseria, M. Robb, J. Cheeseman, G. Scalmani, V. Barone, B. Mennucci, G. Petersson, H. Nakatsuji, M. Caricato, X. Li, H. Hratchian, A. Izmaylov, J. Bloino, G. Zheng, J. Sonnenberg, M. Hada, M. Ehara, K. Toyota, R. Fukuda, J. Hasegawa, M. Ishida, T. Nakajima, Y. Honda, O. Kitao, H. Nakai, T. Vreven, J. Montgomery, J. Peralta, F. Ogliaro, M. Bearpark, J. Heyd, E. Brothers, K. Kudin, V. Staroverov, T. Keith, R. Kobayashi, J. Normand, K. Raghavachari, A. Rendell, J. Burant, S. Iyengar, J. Tomasi, M. Cossi, N. Rega, J. Millam, M. Klene, J. Knox, J. Cross, V. Bakken, C. Adamo, J. Jaramillo, R. Gomperts, R. Stratmann, O. Yazyev, A. Austin, R. Cammi, C. Pomelli, J. Ochterski, R. Martin, K. Morokuma, V. Zakrzewski, G. Voth, P. Salvador, J. Dannenberg, S. Dapprich, A. Daniels, O. Farkas, J. Foresman, J. Ortiz, J. Cioslowski and D. Fox, *Gaussian 09, Revision B.01*, Gaussian, Inc., Wallingford CT, 2010.
31 Parallel Quantum Solutions (PQS), *version 4.0*, Green Acres Road 72703, Arkansas, Fayetteville, 2013, http://www.pqs-chem.com.
32 G. Scuseria, C. Janssen and H. Schaefer, *J. Chem. Phys.*, 1988, **89**, 7382.
33 J. Pople, M. Head-Gordon and K. Raghavachari, *J. Chem. Phys.*, 1987, **87**, 5968.
34 T. Janowski, A. Ford and P. Pulay, *J. Chem. Theory Comput.*, 2007, **3**, 1368.
35 T. Yanai, D. Tew and N. Handy, *Chem. Phys. Lett.*, 2004, **393**, 51.
36 A. Allouche, *J. Comput. Chem.*, 2011, **32**, 174.
37 W. Humphrey, A. Dalke and K. Schulten, *J. Mol. Graphics*, 1996, **14**, 33.
38 Visual Molecular Dynamics (VMD), *version 1.8.9*, http://www.ks.uiuc.edu/Research/vmd/.